Electrical resistivity and structure of liquid Al-Ge alloys

1989 J. Phys.: Condens. Matter 1 2409

(http://iopscience.iop.org/0953-8984/1/13/013)

J. Phys.: Condens. Matter 1 (1989) 2409–2425. Printed in the UK

Electrical resistivity and structure of liquid Al–Ge alloys

Jean-Georges Gasser†, Moussa Mayoufi† and
Marie-Claire Bellissent-Funel‡

† Laboratoire de Physique des Liquides Métalliques, Faculté des Sciences, Ile du Saulcy, 57045 Metz Cédex 1, France

‡ Laboratoire Léon Brillouin§, CEN-Saclay, 91191 Gif-sur-Yvette Cédex, France

Received 19 July 1988, in final form 5 December 1988

Abstract. Aluminium is very reactive with the quartz glass vessel generally used for electrical resistivity measurement cells. In this paper we will describe a new geometrical arrangement to measure accurately the electrical resistivity of liquid alloys, using an alumina vessel. We give our experimental results for the $Al_{1-x}Ge_x$ liquid alloys. This system presents an anomalous concentration-dependent temperature coefficient of the resistivity, with respect to the calculated curves, when using the Faber–Ziman formula with pseudopotential form factors and hard-sphere partial structure factors. We have measured total structure factors of four Al–Ge alloys by neutron scattering on the 'Orphée' reactor at Saclay, using sapphire monocrystal cells. The temperature dependence of the total experimental structure factor explains qualitatively the anomalous resistivity temperature coefficient.

1. Introduction

It is largely agreed that electrical transport in simple metals has been well resolved from a theoretical point of view. In liquid metallic alloys, the transport properties are generally interpreted with the Faber–Ziman formalism [1] in terms of pseudopotentials and structure factors. We recall the basic formula in § 2 together with the parameters used for the practical calculations.

Aluminium is very reactive in the liquid state. Glasses, like quartz glass vessels, react at high temperature and cannot be used to contain liquid aluminium or aluminium alloys. To measure the electrical resistivity, it is necessary to give the liquid a particular geometrical shape and to measure a voltage drop. This is easy to do with a glass (pyrex or quartz), and leak-free cells can be elaborated without major difficulty. This is not the case with alumina which cannot be blown or welded. We elaborate a new experimental design, to measure the electrical resistivity of metals and alloys in an alumina device, conserving the main advantages of our quartz cells. The first one is the possibility of filling the capillary from the bottom in order to avoid the presence of bubbles. The second one is the possibility of changing the composition of the alloy during the experiment. We present the experimental design in § 3 and the experimental results in § 4.

In § 5 we compare our measurements to the calculated results. The composition dependence of the resistivity temperature coefficient presents a minimum near the

§ Laboratoire commun CEA-CNRS.

0953-8984/89/132409 + 17 $02.50

equi-atomic composition, while the Ziman formalism predicts a maximum for all the pseudopotentials used.

The problem is to verify if this discrepancy comes from the Ziman formula, or from its components such as the pseudopotential form factor or the structure factors. We have examined experimentally this last hypothesis.

Pure aluminium presents a very hard-sphere-like structure factor, with about 11.5 nearest neighbours [2], while pure germanium has an important shoulder on the high-angle side of the main peak of the structure factor and has only 6.6 nearest neighbours [3]. It is possible that the transition from a hard-sphere to a shoulder structure factor is accompanied by a particular behaviour which can explain the anomaly in the resistivity temperature coefficient. However aluminium cannot be examined by neutrons in the commonly used quartz cells while metallic cells like vanadium react with germanium. In § 6 we present the experimental design to measure the structure in sapphire monocrystal crucibles. They are oriented in order to minimise the Bragg peaks. The remaining spectrum of sapphire is measured in order to subtract its effect from the total spectrum of the liquid alloy.

Our total experimental structure factors and their temperature dependence are compared to the hard-sphere structure factors. The temperature effect on experimental resistivity is discussed in § 7.

2. Theory

Ziman [4] has shown that the electrical resistivity of a pure liquid metal can be computed using the expression

$$\rho = \frac{3\pi m^2 \Omega_0}{4e^2\hbar^3 k_F^6} \int_0^{2k_F} a(q) v^2(q) q^3 \, \mathrm{d}q$$

where $a(q)$ is the static structure factor, $v(q)$ the pseudo- (or model) potential form factor, Ω_0 the atomic volume and k_F the Fermi wavevector. Other symbols have their customary meaning. This formula can be extended to binary alloys [1] by replacing the product $a(q)v(q)^2$ by

$$[v_1(q)]^2[c(1-c) + c^2 a_{11}(q)] + [v_2(q)]^2[c(1-c) + (1-c)^2 a_{22}(q)] + 2v_1(q)v_2(q)c(1-c)[a_{12}(q) - 1].$$

Here c is the atomic fraction of constituent 1, $v_i(q)$ the form factor of species i in the alloy and the $a_{ij}(q)$ are the Faber–Ziman [5] partial structure factors describing a mixture of randomly distributed hard spheres with different diameters. In this paper we used three local model potentials: the Ashcroft empty core potential (ECP) [6], the Harrison point ion potential (PIP) [7] and the Shaw local optimised model potential (OMP) [8].

These potentials have been discussed by Shaw [8]. We also used the local screened, non-local model potential of Heine–Abarenkov–Animalu [9–11], what Animalu [12] calls the simple model potential (SMP). The parameters used have been taken from the Animalu–Heine [11] paper and the potential form factor has been recalculated at the atomic and electronic density of the liquid alloy with the Vashishta–Singwi [13] dielectric screening function.

To prevent an arbitrary choice of the local model potential parameters, we took the value which gives the same node as the Animalu–Heine non-local screened, non-local

model potential [11]. In a certain sense we have then introduced indirectly first-principle model potentials which include some non-locality through the choice of the parameter. The different parameters are obtained from the relations

$$R_{\mathrm{ECP}} = \pi/2q_0$$

$$R_{\mathrm{OMP}} = \pi/q_0 = 2R_{\mathrm{ECP}}$$

$$\beta = Ze^2/\varepsilon_0 q_0^2$$

where q_0 is the node of the Animalu–Heine non-local model potential [11] ($q_0 = 1.372$ au for aluminium and 1.543 au for germanium). We obtained $R_{\mathrm{ECP}} = 1.145$ au for aluminium and 1.018 au for germanium; $\beta = 40.0$ au for aluminium and 42.2 au for germanium. These parameters are held constant with temperature and concentration in the alloy. The values obtained are near those tabulated by Cohen and Heine [14] and by Harrison [7].

Our calculations have been performed with Ashcroft–Langreth [15] hard-sphere partial structure factors. We chose, as parameters, two hard-sphere diameters for the two species and held them constant with concentration but not with temperature. These hard-sphere diameters have been obtained from the pure metal data. At each temperature, the hard-sphere diameters are deduced from the experimental densities of the pure metals, compiled by Crawley [16], and from the packing fraction given by the Waseda empirical law [17]

$$\eta_i(T) = A_i \exp(-B_i T)$$

where the parameters A_i and B_i have been taken from Waseda's book [2]. The hard-sphere diameters are

$$\sigma_i^3(T) = [6\eta_i(T)\Omega_0(T)/\pi].$$

In the alloy we have taken into account the modification of the mean atomic volume $\Omega_0(T)$ and of the Fermi wavevector k_{F}

$$k_{\mathrm{F}}^3 = [3\pi^2 Z(c)/\Omega_0(T, c)]$$

where $Z(c)$ and $\Omega_0(T, c)$ are respectively the mean valence and the mean atomic volume of the alloy obtained by a linear interpolation of the pure metal values.

3. Experimental method and arrangement of resistivity measurements

Our resistivity quartz cells [18] cannot be used to measure the electrical resistivity of aluminium–germanium alloys. Alumina resistivity cells have even been used before, for instance by Perron [19], for selenium–tellurium alloys, by Kita and Morita [20] for alloys of iron, cobalt and nickel and by Van Zytveld [21] for high-melting pure metals like iron, chromium and platinum.

Constructing a resistivity alumina cell is a difficult problem from a technological point of view. The cells of Perron [19] and Kita [20] used cement between different pieces of alumina for which there is always a problem of tightness relative to liquid and to gases (especially at high temperature). Moreover, the cements are chemically composite materials, and it is necessary that none of them reacts with each metal of the alloy. Kita's principal idea is to use, for an electrode, the transitions of the studied metal

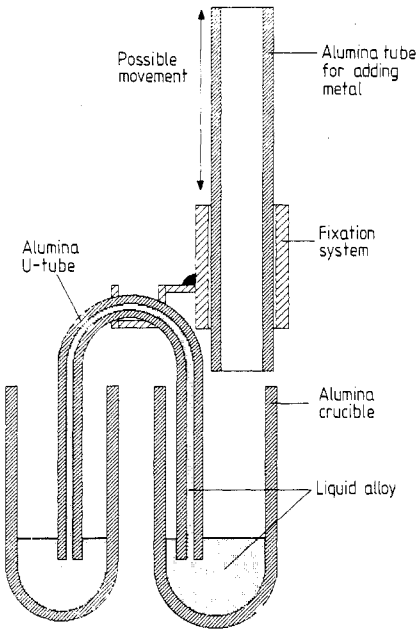

Figure 1. Measurement arrangement.

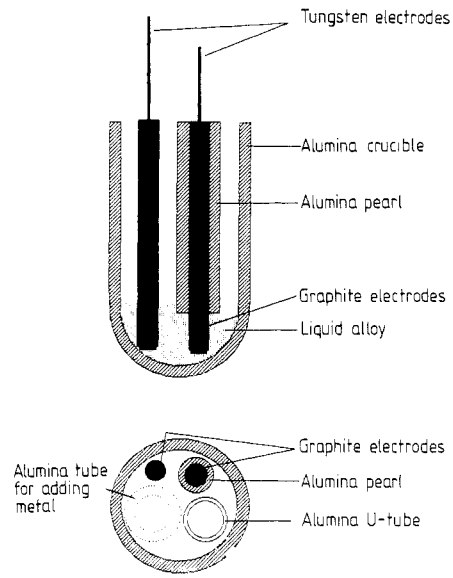

Figure 2. Measurement cell. Details of electrical contacts in each crucible.

from liquid to solid phase. However, this induces errors when one studies alloys which can more or less dissolve the pure metal electrode.

We have realised an experimental design for a vessel without chemical (cement) or mechanical link composed of pure alumina elements. The alumina capillary (like our older quartz cells) is filled from the bottom, pushed up by pressure of argon at about 20 to 50 times the manometric height of the liquid. This ensures that no bubble exists in the capillary. The composition of the studied alloy can be modified during the experimental run.

The measurement cell is represented on figure 1. The principal idea is to use a pure alumina U-tube specially manufactured by the society 'Desmarquest'. All other components can be currently found in alumina catalogues. The whole system has been put in a refractory NS30 stainless-steel tight chamber where vacuum or pressure can be applied. It can be used at up to 1100 °C and will be described later. The alumina U-tube can be moved up and down and the capillary can then be cleared and filled again. Two alumina tubes permit the adding of metal in the two crucibles in order to modify the composition. The geometrical constant of the cell was calibrated by measuring the resistivity of triple-distilled mercury.

When an experimental run is begun, the capillary U-tube is placed in a low position. Weighed pieces of the metals are put in the two crucibles. The whole arrangement is heated under secondary vacuum until the metals are melted. An absolute pressure of argon of 1–3 bar is then applied over the liquid sample and pushes the liquid alloy into the capillary tube.

The resistivity is measured by a four-probe method. In each crucible, two tungsten wires are 'picked' in graphite electrodes. The details are represented on figure 2. The whole arrangement (figure 3) is hung from the head with chromel wires and put in a

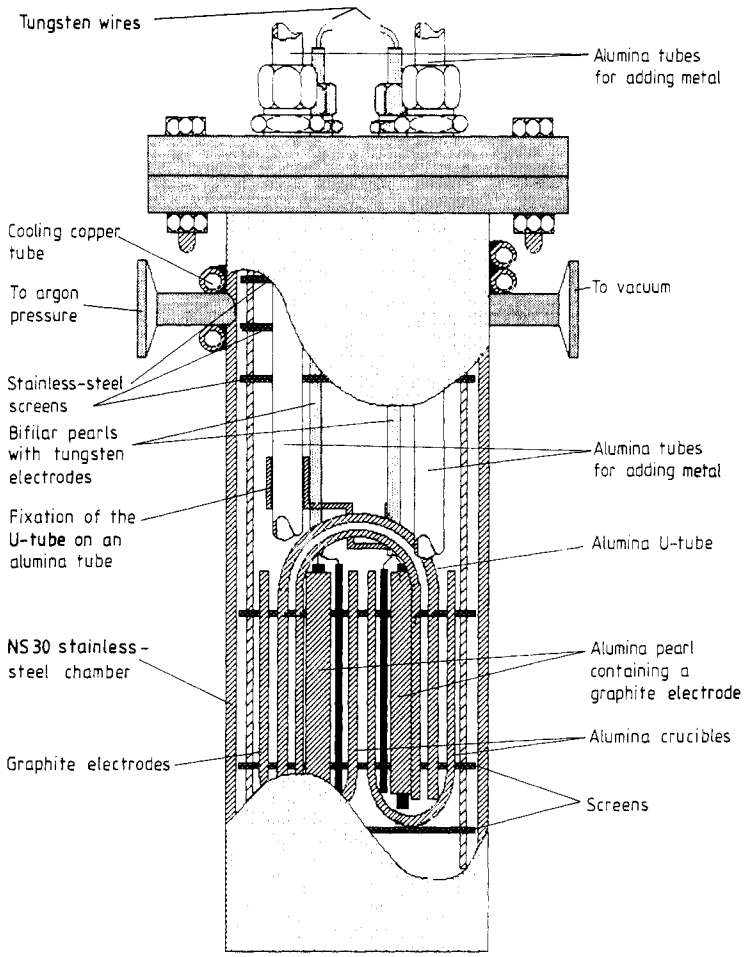

Figure 3. Measurement system in a stainless-steel enclosure.

stainless-steel enclosure. The upper part is cooled by water. Only the lowest part is heated. The head, at laboratory temperature, is fixed with screws. An absolute pressure of 3 bar can be applied. The tightness is realised with an O-ring. The arrangement has been tested up to 1100 °C.

It is possible to replace the stainless-steel tube by an alumina tube. The head must then be modified but the principle of the experimental arrangement can be conserved. It will then be possible to make experiments at higher temperature (~1800 °C).

A stable constant current is furnished by a General Resistance DIAL DAS 86 generator. The voltage drop is measured with a 1 μV resolution 120000 points Hewlett Packard 3490 voltmeter. Thermoelectric EMF are eliminated by inverting the current. The accuracy of the electrical resistivity is estimated to 0.4%, that of the composition of the alloy to 0.3 at.% and that of the temperature to 0.3%.

4. Experimental resistivity

The phase diagram of the Al–Ge system is represented on figure 4 [22]. It presents a eutectic temperature of 424 °C at 30 at.% Ge.

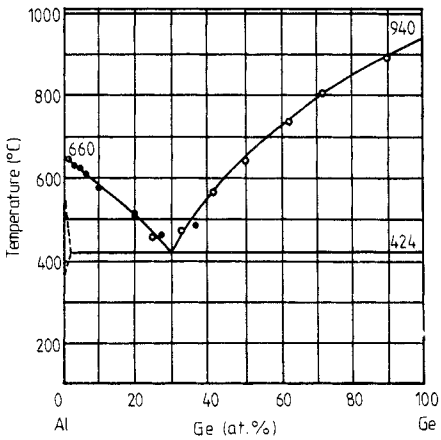

Figure 4. Phase diagram of the Al–Ge system (after Hansen [22]).

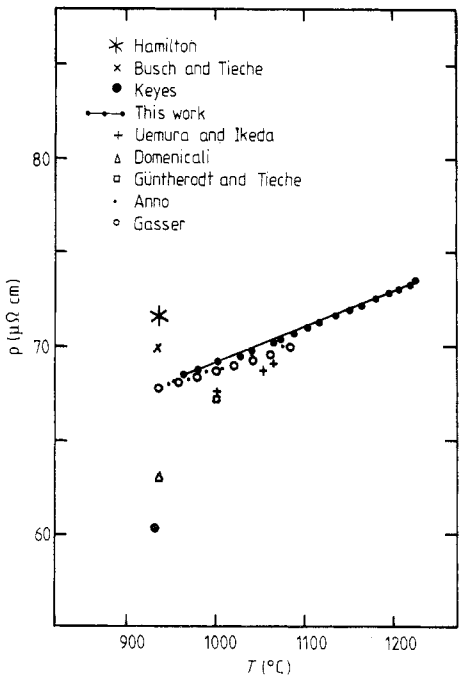

Figure 5. Electrical resistivity of pure liquid germanium.

4.1. Pure germanium

The electrical resistivity of pure liquid germanium is represented on figure 5, together with values from other authors. It has been measured from the melting point to 1220 °C. Earlier measurements are very dispersed around our values. At the melting point all measurements made in our laboratory [23, 24] converge to a value of 67.8 $\mu\Omega$ cm. At higher temperatures, we obtain a small difference (0.4% with Anno [23] at 1080 °C; 0.5% with Gasser [24] at the same temperature).

Only Uemura and Ikeda [25] gave a temperature dependence curve. Their resistivity value is 2% below ours at 1000 °C. The temperature coefficient is about 16.3 nΩ cm K^{-1} while ours grows from 13.0 at the melting point to 15.8 nΩ cm K^{-1} at 1200 °C. Other values are only given at the melting point. Hamilton and Seidensticker [26] and Busch and Tieche [27] are respectively 5.3% and 3.2% higher; Domenicali [28] and Keyes [29] respectively 7.1% and 11.5% lower than our value at the melting point.

4.2. Pure aluminium

The electrical resistivity of liquid aluminium has been measured from the melting point to 1050 °C. Our results are represented on figure 6 together with values of other authors. The value at the melting point is 24.36 $\mu\Omega$ cm. The electrodeless method used by Roll and Motz [30] and by Keita *et al* [31] give respectively 2% more and 6.4% less than our value at the melting point. The electrode technique of Matuyama [32], Rowdo [33] and Batalin [34] gives respectively 6.7% and 3.2% more, and 0.3% less than our values. The accuracy of our measurements is estimated to 0.15 $\mu\Omega$ cm.

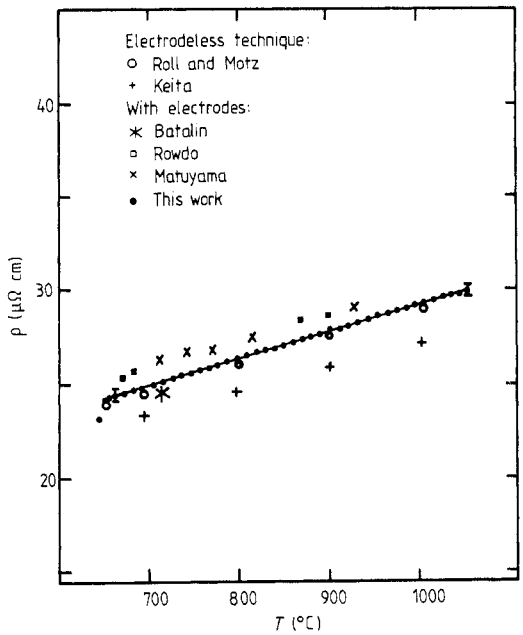

Figure 6. Electrical resistivity of pure liquid aluminium.

4.3. Aluminium–germanium alloys

To our knowledge, the electrical resistivity of Al–Ge alloys has never been published before. Our experimental results are represented on figure 7 as a function of temperature. The scatter of the values is small (0.1 $\mu\Omega$ cm) except for $Al_{70}Ge_{30}$ where it attains 0.4 $\mu\Omega$ cm. We obtain the same results with rising or lowering temperature. The resistivity varies linearly with temperature, except near the eutectic concentrations.

5. Interpretation and discussion

5.1. Pure metals

5.1.1. Liquid germanium. The electrical resistivity of liquid germanium has been calculated at 1000 °C with respectively the OMP, the ECP, the SMP and the PIP potentials, and compared to the experimental resistivity (69.0 $\mu\Omega$ cm). We obtained respectively 27.7 (−60%), 44.6 (−35%), 47.0 (−32%) and 60.3 $\mu\Omega$ cm (−12%). For all the model potentials, the resistivity is underestimated.

5.1.2. Liquid aluminium. The calculated electrical resistivities of aluminium at 1000 °C with respectively the OMP, ECP, SMP and PIP potentials are 12.8 (−56%), 29 (−1.7%), 25.7 (−13%) and 48.6 $\mu\Omega$ cm (+64%) compared to the experimental value of 29.5 $\mu\Omega$ cm. The results can be considered as good with the ECP and the SMP. In all cases the local OMP underestimates the resistivity. It can be explained by the fact that the optimisation procedure reduces the oscillations of the form factor which is the smallest one at the limit of integration $2k_F$. With the PIP the $2k_F$ value of the form factor is too important for aluminium.

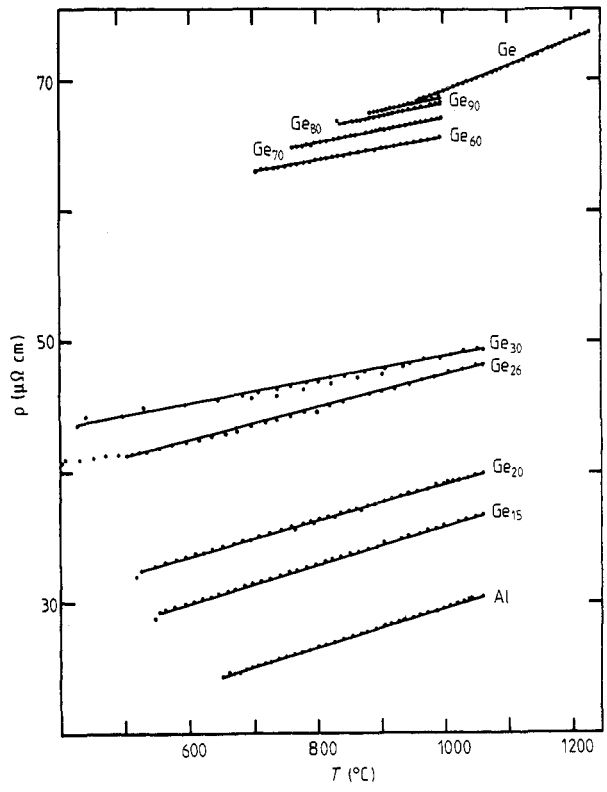

Figure 7. Electrical resistivity of ten liquid Al_{1-x}–Ge_x alloys.

The remaining discrepancies may be explained by four reasons:
(i) the structure factor is not correctly described by hard spheres;
(ii) the dielectric screening function does not describe correctly the screening;
(iii) the bare potentials are not good ones; and
(iv) the Ziman formula is incorrect.

The first reason could apply to liquid germanium. In order to measure this effect, we have calculated the resistivity with the experimental structure factor of germanium, tabulated by Orton and Woodisse [35]. We obtained with the SMP potential a resistivity of 51.5 $\mu\Omega$ cm (−25%), 7% better than with hard spheres.

The influence of the dielectric screening function has been studied by Gasser [18] for liquid sodium, but the results are identical for the other metals (unpublished work). The resistivity can vary by a factor of 2.5 following the dielectric screening function chosen, but those considered as the 'best ones' (Vashishta–Singwi [13], Toigo–Woodruff [36]) give nearly the same result.

The bare potentials can also be suspect. However if there is some arbitrariness in the choice of the parameter of local model potentials (OMP, PIP, ECP) it is less so if we use a first-principle non-local model potential like the SMP. Animalu [12] has shown that the effect of non-local screening on these potentials does not modify the resistivity by more than 3% for liquid aluminium.

The Ziman formula is a first-order expression for the resistivity of liquid metals. Multiple scattering is neglected. The Ziman formula can however be corrected by introducing an effective-mass correction which also affects the screening. Very soph-

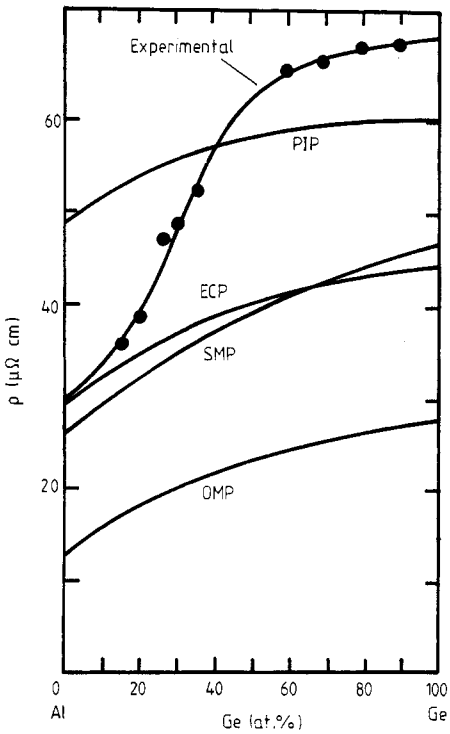

Figure 8. Isotherm of the experimental resistivity of Al_{1-x}–Ge_x at 1000 °C compared to calculated curves with the Ashcroft (ECP), Shaw local (OMP), Harrison (PIP) and Heine–Abarenkov–Animalu local screened, non-local model potential (SMP) and with the Ashcroft–Langreth (AL) hard-sphere partial structure factors.

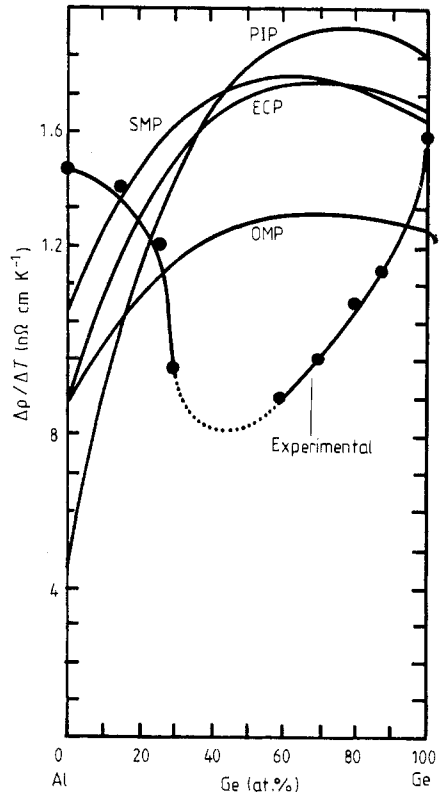

Figure 9. Experimental temperature coefficient of Al_{1-x}–Ge_x at 1000 °C compared to calculated curves with the OMP, ECP, PIP and SMP model potentials and the AL hard-sphere partial structure factors.

isticated non-local model potentials like those proposed by So *et al* [35] give resistivities very near the experimental value even with high-valency and high-atomic-number metals like Pb.

In conclusion, we feel that a trivalent metal like aluminium is well described by the SMP potential and by hard spheres, while germanium cannot be described by a hard-sphere structure factor (but the effect on the resistivity is small). The pseudopotential (and the Ziman formula) must probably be corrected by effective masses.

5.2. Aluminium–germanium alloys

The isotherm of the resistivity at 1000 °C is plotted on figure 8. A very sharp increase is noticed on the aluminium-rich side of the phase diagram, while on the germanium-rich side the resistivity remains nearly constant. The calculated resistivity of the alloy has also been represented with OMP, SMP, ECP and PIP potentials. In all cases, the calculated curves are monotonically convex while the experimental one is sigmoidal.

The temperature coefficient of the resistivity at 1000 °C has been reported on figure 9. The experimental curve presents a minimum near the equi-atomic concentration while all calculated curves are convex and present a maximum.

A minimum in metallic alloys generally occurs when the limit of integration $2k_F$ in the Faber–Ziman formula [1, 38] lies in the main peak. This is the case when the mean valency is about 1.7, i.e. for alloys of polyvalent with monovalent (noble, alkaline, or transition) metals. This classical explanation of temperature coefficient minimum cannot be used for Al–Ge systems.

Aluminium–germanium thermodynamic properties have been studied by Predel and Stein [39]. A large negative enthalpy of mixing has been measured for Al–Ge alloys (-948 cal mol^{-1}). It indicates heteropolar bonding character with a marked tendency towards compound formation. However, the difference in electronegativity being small, the formation of a valence compound having a unique lattice is not possible.

On the other hand, Kahl and Hafner [38], starting from the ECP, with an R_c parameter of 1.12 and 1.03 for respectively aluminium and germanium and with the Ichimaru–Utsumi [39] screening function, calculated the effective inter-atomic potentials and then, for the first time with the optimised random-phase approximation (ORPA), the partial structure factors of alloy. Taking into account the neutron scattering factor of the aluminium and germanium, they constructed the total structure factor as it can be observed with neutrons. A particular result of their calculation was a double-shouldered main peak of the structure factor in the middle of the phase diagram.

It becomes particularly interesting to measure the total structure factor of Al–Ge alloys in order to verify the validity of the ORPA calculations, and to explain the anomaly in the resistivity temperature coefficient.

6. Experimental design for neutron scattering measurements

The neutron diffraction study was performed using the two-axis diffractometer 7C2 built on one of the two beams from the hot source, at the reactor 'Orphée' of the Laboratoire Léon Brillouin at Saclay. The wavelength used was 0.707 Å. The detector was a BF3 multi-detector consisting of 640 cells at an angular distance of 0.2°. The spectrometer has been described by Ambroise and Bellissent [42].

Liquid alloys were studied using single-crystal sapphire crucibles. Sapphire produces Bragg peaks, so it was necessary by a rotation of the crucible, to find an angular position where no peak appears in the angular domain (0 to 128°).

First, a rotation of the crucible of 180° by 0.5° steps is made, very short spectra are taken and analysed automatically† giving the mean value, the height of the peaks and their angular value. It gives us generally four or five angular regions without important peaks. Then short spectra are measured and plotted. The best angular position is chosen. Finally long spectra of the empty crucible are taken. The background, the furnace, the empty container effects, self-absorption and multiple scattering contributions are corrected according to conventional procedures [43].

On figure 10 we have represented spectra of the furnace, of the empty container and of the liquid alloy.

† The automatic analysis has been performed by Alain Menelle.

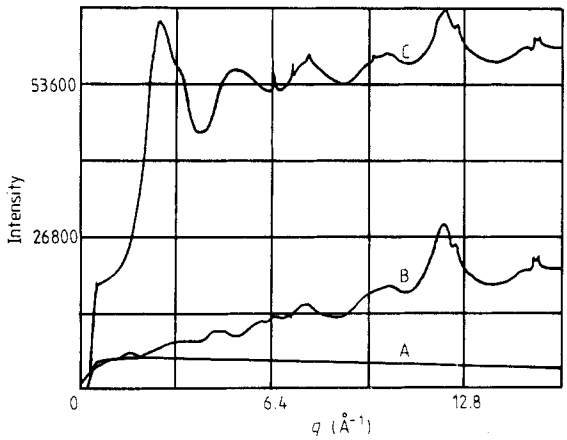

Figure 10. Neutron spectra, at 977 °C, of the empty furnace (curve A), of the empty sapphire container (curve B) and of the liquid alloy in the container (curve C).

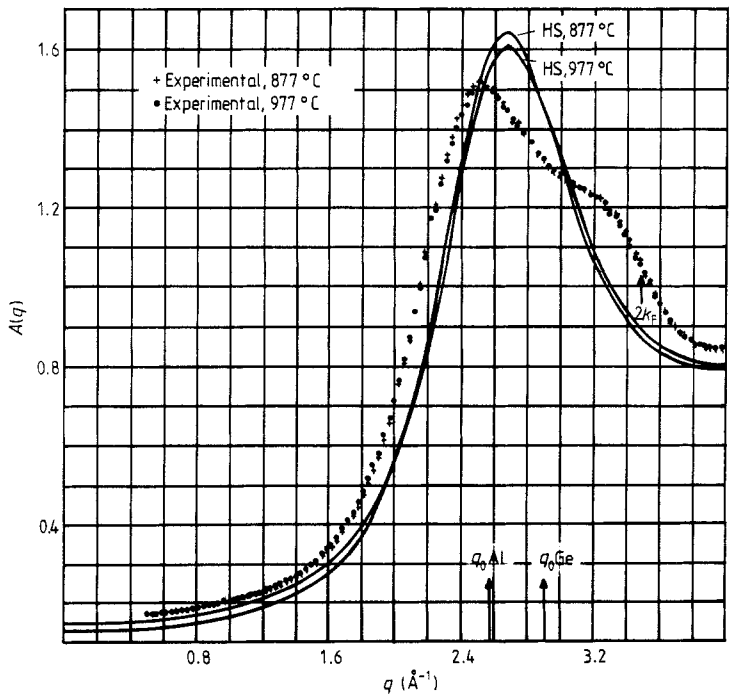

Figure 11. Experimental and (neutron-weighted) hard-sphere total structure factors of Al_{20}–Ge_{80} at 877 and 977 °C. The arrows noted q_0Al and q_0Ge indicate the nodes of the form factors. The arrow noted $2k_F$ indicates that value.

7. Structural results; discussion

On figures 11, 12, 13 and 14, we have represented the structure factors with respectively 80, 60, 40 and 20 at.% germanium between 0 and 4 $Å^{-1}$. At each concentration, measurements have been made at two temperatures, one at 977 °C (1250 K) and another just above the liquidus (at respectively 877, 750, 600 and 550 °C). We have also plotted the computed hard-sphere (neutron-weighted) total structure factor. The hard-sphere

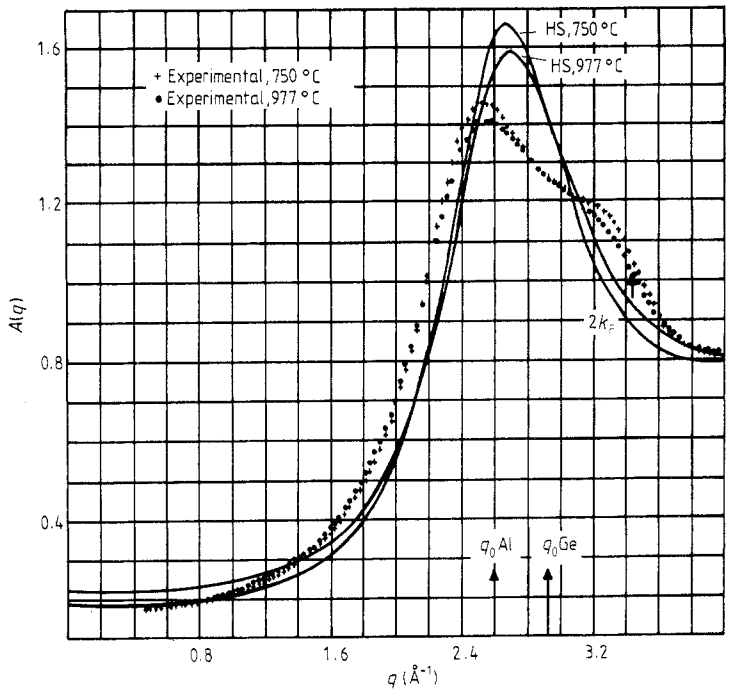

Figure 12. Experimental and (neutron-weighted) hard-sphere total structure factors of Al_{40}–Ge_{60} at 750 and 977 °C. The arrows noted q_0Al and q_0Ge indicate the nodes of the form factors. The arrow noted $2k_F$ indicates that value.

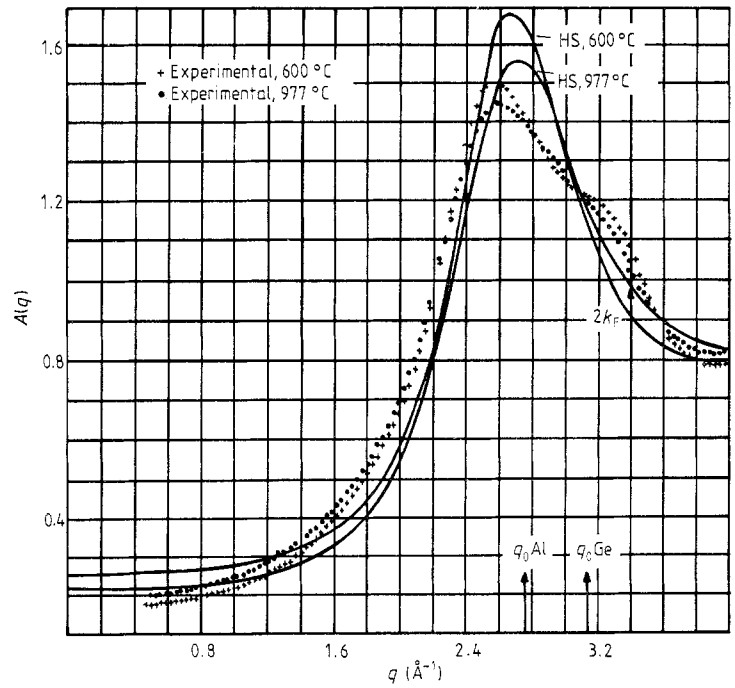

Figure 13. Experimental and (neutron-weighted) hard-sphere total structure factors of Al_{60}–Ge_{40} at 600 and 977 °C. The arrows noted q_0Al and q_0Ge indicate the nodes of the form factors. The arrow noted $2k_F$ indicates that value.

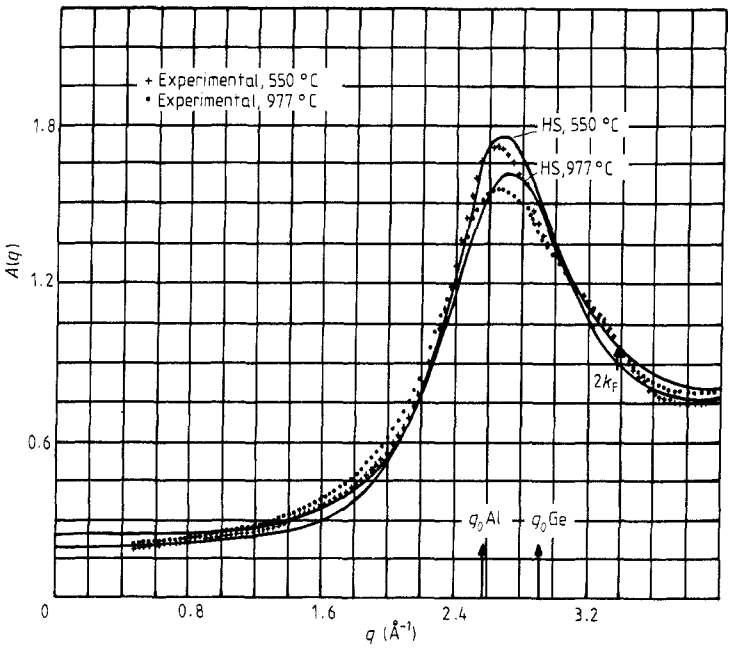

Figure 14. Experimental and (neutron-weighted) hard-sphere total structure factors of Al_{80}–Ge_{20} at 550 and 977 °C. The arrows noted q_0Al and q_0Ge indicate the nodes of the form factors. The arrow noted $2k_F$ indicates that value.

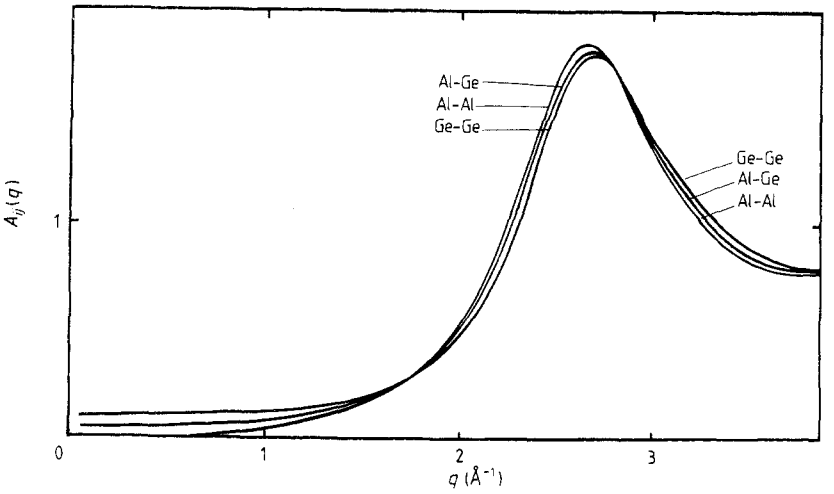

Figure 15. Hard-sphere partial structure factors of Al_{60}–Ge_{40} at 977 °C.

diameters, obtained in the manner described before, are respectively 2.409 Å for germanium and 2.471 Å for aluminium at 977 °C. The neutron weighting factors used are 0.8193 for germanium and 0.3449 for aluminium.

As can be observed on figure 15 the hard-sphere partial structure factors are very similar in height and in the position of their main peak; so that total structure factor

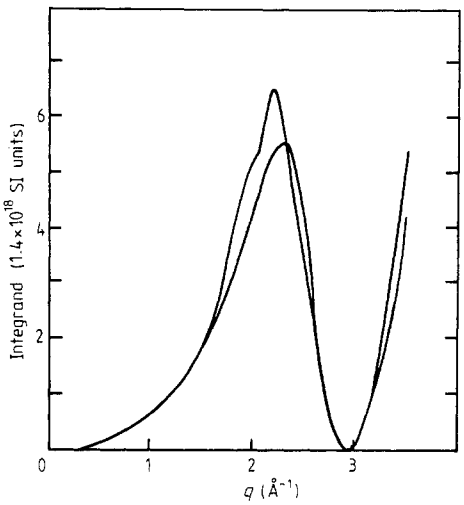

Figure 16. Integrand of the resistivity of pure liquid germanium with the SMP model potential. The higher curve corresponds to the experimental structure factor and the lower to the hard-sphere one.

hump cannot be explained by the combination of the partial structure factors. The hard-sphere total structure factor (figures 11 to 14) looks also like a hard-sphere one.

The interesting feature in figures 11 to 14 is the progressive evolution from the characteristic shouldered structure factor of germanium, with 6.6 nearest neighbours, to the hard-sphere-like structure of aluminium, with 11.5 nearest neighbours. The double-shouldered structure main peak obtained by Kahl and Hafner [40] from the Ashcroft pseudopotential through the ORPA method could not be observed experimentally. More first-principle theoretical work seems necessary for the correct interpretation of the structure factor of alloys.

If we return to the resistivity, the Faber–Ziman formula [1] gives us an integral from 0 to $2k_F$ of the product of the structure factor times the squared form factor, times the wavevector to power 3. The limit of integration $2k_F$ goes from 3.30 to 3.50 $Å^{-1}$ from pure aluminium to pure germanium. The variation is small and we can observe that $2k_F$ is always at the right side of the main peak of the structure factor at a value where $a(q)$ is near one.

The node of the form factor is 2.592 $Å^{-1}$ for aluminium and 2.917 $Å^{-1}$ for germanium. It plays a very important role in the electronic properties. On figure 16 we have plotted the integrand of the resistivity with the SMP potential for pure germanium. As can be seen, two important contributions to the resistivity come from the region before the node, which generally corresponds to the peak of the structure factor, and just below $2k_F$ heavily weighted by the term q^3.

Two features cannot be explained by the Faber–Ziman formula [1] using hard spheres:

(i) the S-like curve of resistivity versus concentration (figure 8); and

(ii) the temperature coefficient of the resistivity (TCR) versus concentration (figure 9).

We have represented on the same graph the measured structure factor of the 80 and the 40 at.% germanium alloy (figure 17) together with the position of the node of the form factors and of the values of $2k_F$. The corresponding hard-sphere structure factor curves are represented in figure 18. They are very similar except in the low-q region where the

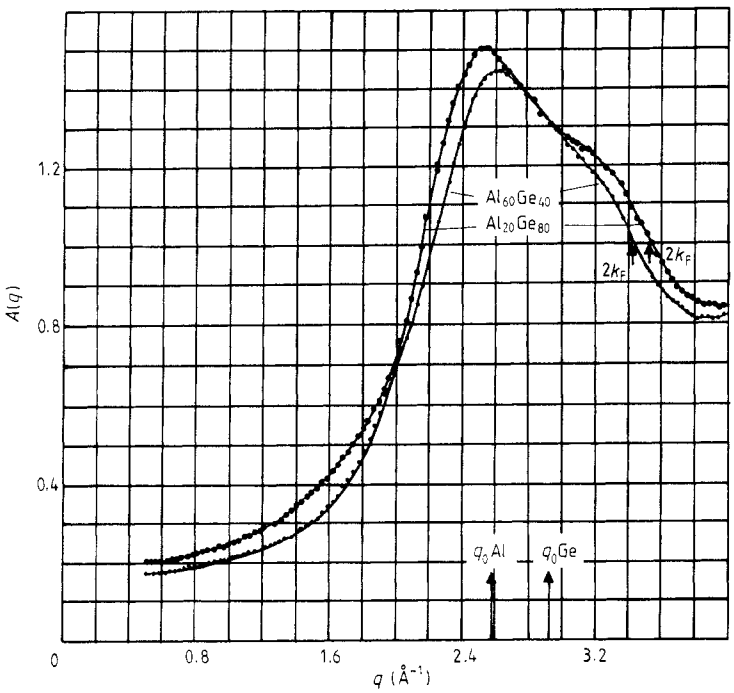

Figure 17. Evolution of the total experimental structure factor of Al_{1-x}–Ge_x liquid alloy at 977 °C when the concentration of germanium is lowered from 80 to 40 at.%.

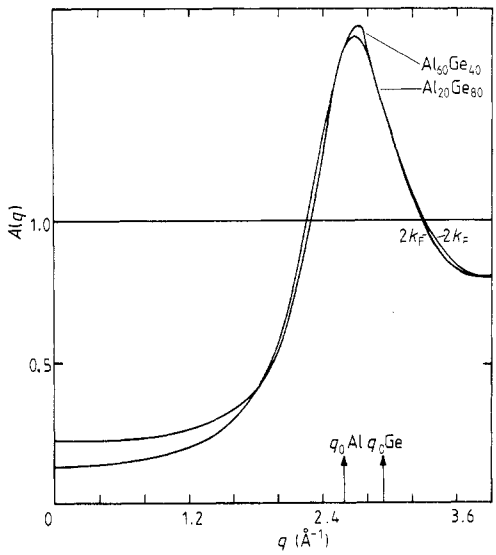

Figure 18. Evolution of the total hard-sphere structure factor of Al_{1-x}–Ge_x liquid alloy when the concentration of germanium is lowered from 80 to 40 at.%.

effect on the resistivity is negligible. The adding of germanium raises the limit of integration. If we examine the experimental structure factors (figure 17), the effect on k_F is already present, but we also observe a sensitive displacement of the main peak to the left, increasing the contribution to the resistivity below the node, and an increase of

the structure factor near $2k_F$. The two contributions are heavily weighted by q^3, explaining why the resistivity grows faster with the concentration in germanium in the real case than with hard spheres.

We will show if the anomaly in the concentration dependence of the temperature coefficient of the resistivity can also be explained by the experimental structure factors. We must return to the Ziman explanation of this effect. When the temperature is raised, the disorder increases and the structure factor tends to unity. Schematically, the temperature coefficient is governed by four contributions. A contribution to a positive coefficient by the low-q region where $a(q)$ is lower than 1; a negative contribution in the peak region; a positive one near the first minimum of the structure factor; and again a negative one because the limit of integration $2k_F$ decreases with temperature. Of course, the position of the node of the form factor modulates these contributions. This explains why monovalent (and noble) metals have a positive temperature coefficient, why some divalent metals have a negative one (zinc) or zero (cadmium) and why the tri-, quadri- and pentavalent ones have a positive one. For an alloy, the TCR is negative (or minimum) when the mean valency is about 1.7.

This classical explanation does not allow the interpretation of the minimum of the TCR of Al–Ge when the hard-sphere partial structure factors are used. However, examination of figures 11 to 14 shows that the temperature dependence of the experimental structure factors is very different from the hard-sphere ones. The first maximum of the experimental structure factor lies at a lower q-value. The negative contribution to the resistivity due to the first peak is minimised with hard-sphere structure factors by the node of the form factors (peak at 2.7 $Å^{-1}$, nodes at 2.6 and 2.9 $Å^{-1}$) while, for example, for 60 at.% Ge (figure 12) the experimental structure factor has a maximum at 2.5 $Å^{-1}$.

A second contribution to the TCR comes from the important variation of the shoulder just below $2k_F$ (see for example figures 12 and 13). The observation of the experimental structure factors shows that at lower temperatures in the middle of the phase diagram (figures 12 and 13) the shoulder is relatively more marked than for the germanium-rich alloy (figure 11). Hence, the temperaure dependence is more important. The most remarkable effect is the inversion in the temperature dependence of the total structure factor *near* $2k_F$ (figures 12 and 13). Indeed the higher-temperature hard-sphere structure factor has greater values just below $2k_F$ while the situation is inverted for the experimental total structure factor. This explains very clearly the anomalous resistivity temperature coefficient of this system *in the framework of Faber–Ziman formula.*

8. Conclusions

We have presented a new experimental design to measure the electrical resistivity of highly reactive liquid alloys. This system has been tested in a stainless-steel chamber up to 1100 °C. It can be adapted to higher temperatures by use of other refractory materials like alumina or sillimanit tube. At Saclay, we have (with other experimentalists) made our measurements with a new experimental system using a previously oriented sapphire monocrystal crucible. A full experimental study on Al–Ge alloys has been made by measuring simultaneously the electrical resistivity and the total structure factor. It has been shown that the Faber–Ziman formalism [1] does not allow the interpretation of the experimental resistivity, if hard-sphere structure factors are used. However, the experimental structure factors explain qualitatively the anomalous feature of the res-

istivity. Further progress can come from further first-principle calculations of total structure factor like Kahl and Hafner's work, which must however be improved.

References

[1] Faber T E and Ziman J M 1965 *Phil. Mag.* **11** 153
[2] Waseda Y 1980 *The Structure of Non-Crystalline Materials* (New York: McGraw-Hill) table 3-1, p 54
[3] Bellissent-Funel M C and Bellissent R 1984 *J. Non-Cryst. Solids* **65** 38
[4] Ziman J M 1961 *Phil. Mag.* **6** 1013
[5] Faber T E 1972 *Introduction to the Theory of Liquid Metals* (Cambridge: CUP)
[6] Ashcroft N W 1966 *Phys. Lett.* **23** 48
[7] Harrison W A 1966 *Pseudopotentials in the Theory of Metals* (New York: Benjamin)
[8] Shaw R W 1972 *Phys. Rev.* B **5** 4742
[9] Heine V and Abarenkov I V 1964 *Phil. Mag.* **9** 451
[10] Abarenkov I V and Heine V 1965 *Phil. Mag.* **12** 522
[11] Animalu A O E and Heine V 1965 *Phil. Mag.* **12** 1249
[12] Animalu A O E 1973 *Phys. Rev.* B **8** 3542
[13] Vashishta P and Singwi K S 1972 *Phys. Rev.* B **6** 875
[14] Cohen M L and Heine V 1970 *Solid State Phys.* **24** 38
[15] Ashcroft N W and Langreth D C 1967 *Phys. Rev.* **156** 685
[16] Crawley A F 1974 *Int. Met. Rev.* **19** 32
[17] Waseda Y 1980 *The Structure of Non-Crystalline Materials* (New York: McGraw-Hill)
[18] Gasser J G 1982 *Thèse de Doctorat d'Etat* Université de Metz
[19] Perron J C 1969 *Thèse de Doctorat d'Etat* Université de Paris
[20] Kita Y and Morita Z 1984 *J. Non-Cryst. Solids* **61 & 62** 1079
[21] Van-Zytveld J B 1984 *J. Non-Cryst. Solids* **61 & 62** 1085
[22] Hansen M 1958 *Constitution of Binary Alloys* (New York: McGraw-Hill)
[23] Anno L 1985 *Mémoire d'ingénieur CNAM* Université de Metz
[24] Gasser J G and Muller J D 1980 *NATO Summer School* ed Lüscher and Coufal (Sijthoff & Nordhoff) p 631
[25] Uemura O and Ikeda S 1973 *Trans. Japan. Inst. Met.* **14** 351
[26] Hamilton P R and Seidensticker R C 1963 *J. Appl. Phys.* **34** 2697
[27] Busch G and Tieche Y 1963 *Phys. Kond. Mater.* **1** 78
[28] Domenicali C A 1957 *J. Appl. Phys.* **28** 749
[29] Keyes R W 1951 *Phys. Rev.* **84** 267
[30] Roll A and Motz H 1957 *Z. Metallk.* **48** 272
[31] Keita M, Steinemann S, Künzi H U and Güntherodt H J 1977 *Liquid Metals 1976* (Inst. Phys. Conf. Ser. 30) p 655
[32] Matuyama Y 1927 *Sci. Rep. Tohoku Univ.* **16** 447
[33] Rowdo 1981 *Mémoire d'ingénieur CNAM* Université de Metz
[34] Batalin G I and Khakonov A I 1970 *Fiz. Met. Metall.* **29** 113
[35] Orton B R and Woodisse S P 1973 *J. Phys. F.: Met. Phys.* **3** 1141
[36] Toigo F and Woodruff T O 1970 *Phys. Rev.* B **2** 3958
[37] So C B, Moore R A and Wang S 1978 *J. Phys. F: Met. Phys.* **8** 785
[38] Busch G and Güntherodt H J 1974 *Solid State Phys.* **29** 235
[39] Predel B and Stein D W 1971 *Z. Metallk.* **62** 499
[40] Kahl G and Hafner J 1988 *Z. Phys. Chem.* **156** 645
[41] Ichimaru S and Utsumi K 1981 *Phys. Rev.* B **24** 7385
[42] Ambroise J P and Bellissent R 1982 *Workshop on the Position Sensitive Detection of Thermal Neutrons* ILL, Grenoble
[43] Bellissent M C 1977 *Thèse de Doctorat d'Etat* Université de Grenoble
[44] Güntherodt H J and Tieche Y 1978 *Helv. Phys. Acta* **41** 855